Journal of the Geological Society, London, Vol. **162**, 2005, pp. 1–10. Printed in Great Britain.

U–Pb SIMS dating of synkinematic granites: timing of core-complex formation in the northern Anatolide belt of western Turkey

UWE RING[1] & ALAN S. COLLINS[2]

[1]*Institut für Geowissenschaften, Johannes Gutenberg-Universität, 55099 Mainz, Germany (e-mail: ring@uni-mainz.de)*

[2]*Tectonics Special Research Centre, School of Earth and Geographical Sciences, The University of Western Australia, Crawley, WA 6009, Australia*

Abstract: Secondary ion mass spectrometry (SIMS) U–Th–Pb dating of magmatic zircon from the synkinematic Eğrigöz and Koyunoba granites and a leucogranite dyke dates core-complex formation in the northern Anatolide belt of western Turkey at 24–20 Ma. The granites intrude into the footwall of the Simav detachment and are strongly elongated in the NNE direction parallel to tectonic transport on the detachment. Although large parts of the granites are undeformed, localized mylonitic to ultramylonitic deformation occurs directly beneath the Simav detachment and preserves evidence of progressive deformation from ductile to brittle conditions. Oscillatory zoned rims of long-prismatic zircon from the Eğrigöz and Koyunoba granites yield identical and well-constrained intrusion ages of 20.7 ± 0.6 Ma and 21.0 ± 0.2 Ma, whereas inherited grains range from Palaeoproterozoic (2972 ± 13 Ma) to Neoproterozoic (653 ± 6 Ma to 500 ± 5 Ma) in age. A leucogranite dyke yields an intrusion age of 24.4 ± 0.3 Ma, with inherited Neoproterozoic (640 ± 7 Ma to 511 ± 6 Ma) grains. Our data, in conjunction with published $^{40}Ar/^{39}Ar$ biotite ages, indicate very rapid cooling (greater than *c*. 200 °C Ma^{-1}) for the granites during and after synkinematic emplacement.

Keywords: U–Pb, Anatolide belt, detachment faults, metamorphic core complexes, granites.

Synkinematic granites are important for dating orogenic processes and thus for understanding the evolution of mountain belts. A close relationship between granite emplacement and movement along major extensional detachments has been documented (Coney 1980; Gans *et al*. 1989; Hill *et al*. 1992; Lee & Lister 1992), hence such a relationship helps to constrain the age of the detachments. The Anatolide belt of western Turkey exposes remarkable late-orogenic extensional detachments (Bozkurt 2000; Gessner *et al*. 2001*a*; Işik & Tekeli 2001; Seyitoğlu *et al*. 2002; Işik *et al*. 2004). A bivergent system of Pliocene to Recent detachments bounds the Central Menderes metamorphic core complex (Gessner *et al*. 2001*a*) (Fig. 1). Towards the margins of the Anatolide belt, detachment faulting appears to be older (Seyitoğlu *et al*. 1992; Işik & Tekeli 2001; Ring *et al*. 2003*a*; Işik *et al*. 2004) but the exact timing of core-complex formation is not well constrained.

We report Late Oligocene to Early Miocene secondary ion mass spectrometry (SIMS) U–Th–Pb zircon ages of 20.7 ± 0.6 Ma from the Eğrigöz granite, 21.0 ± 0.2 Ma for the Koyunoba granite and 24.4 ± 0.3 Ma (all 2σ errors) for a leucogranite dyke, and demonstrate the coeval relationship between movement of the Simav detachment and these synkinematic intrusions. In conjunction with one recently reported $^{40}Ar/^{39}Ar$ white mica age of 22.9 ± 0.5 Ma for mylonitization of a pre-shear-zone rock (Işik *et al*. 2004) this constrains the timing of core-complex formation at the northern margin of the Anatolide belt of western Turkey.

Setting

Previous research revealed that the architecture of the Anatolide belt in western Turkey comprises three major tectonometamorphic units, which are characterized by different lithologies, protolith ages, pre-collisional palaeogeography and orogenic history (Ring *et al*. 1999*a*). This heterogeneous tectonic pile was assembled during Eocene collision-related crustal shortening (Gessner *et al*. 2001*c*). The Lycian Nappes and the Vardar–İzmir–Ankara suture zone represent the upper tectonometamorphic unit, both of which were high-pressure metamorphosed and deformed in the Late Cretaceous (before *c*. 75 Ma) (Collins & Robertson 1997, 1998; Sherlock *et al*. 1999; Oberhänsli *et al*. 2001;Ring & Layer 2003). The middle tectonometamorphic unit has been correlated with the Cycladic blueschist unit in the Aegean (Candan *et al*. 1997; Ring *et al*. 1999*a*). The Menderes nappes make up the lower tectonometamorphic unit and, unlike the other two, do not show Late Cretaceous to Eocene high-pressure metamorphism. The high-pressure rocks of the middle and upper tectonometamorphic units are separated from the Menderes nappes by a huge out-of-sequence thrust, the Eocene Cyclades–Menderes thrust (Gessner *et al*. 2001*c*) (Fig. 1).

After Late Cretaceous to Eocene crustal shortening, the Anatolide belt underwent at least two periods of extensional faulting. In the northern part of the Anatolide belt, Işik & Tekeli (2001) and Işik *et al*. (2004) identified the top-to-the-NNE Simav detachment (Fig. 2). The Simav detachment reactivated the Eocene Cyclades–Menderes thrust so that the rocks of the Cycladic blueschist unit and the Vardar–İzmir–Ankara zone make up the hanging wall of the detachment. The footwall consists of Precambrian gneiss of the Menderes nappes. Locally this gneiss is caught up in the detachment zone and occasionally occurs in a hanging-wall position. The Eğrigöz and Koyunoba granites, and also the Alaçam granite further west, the Demirçi granite further south (Fig. 1) and a number of smaller granites and granitic dykes, intruded into footwall gneiss. The timing of movement on the Simav detachment is not well constrained, but is thought to be older than a 16–15 Ma volcano-sedimentary sequence that unconformably overlies the detachment (Seyitoğlu *et al*. 1992; Işik & Tekeli 2001). Apatite fission-track ages of

Article number = 04016

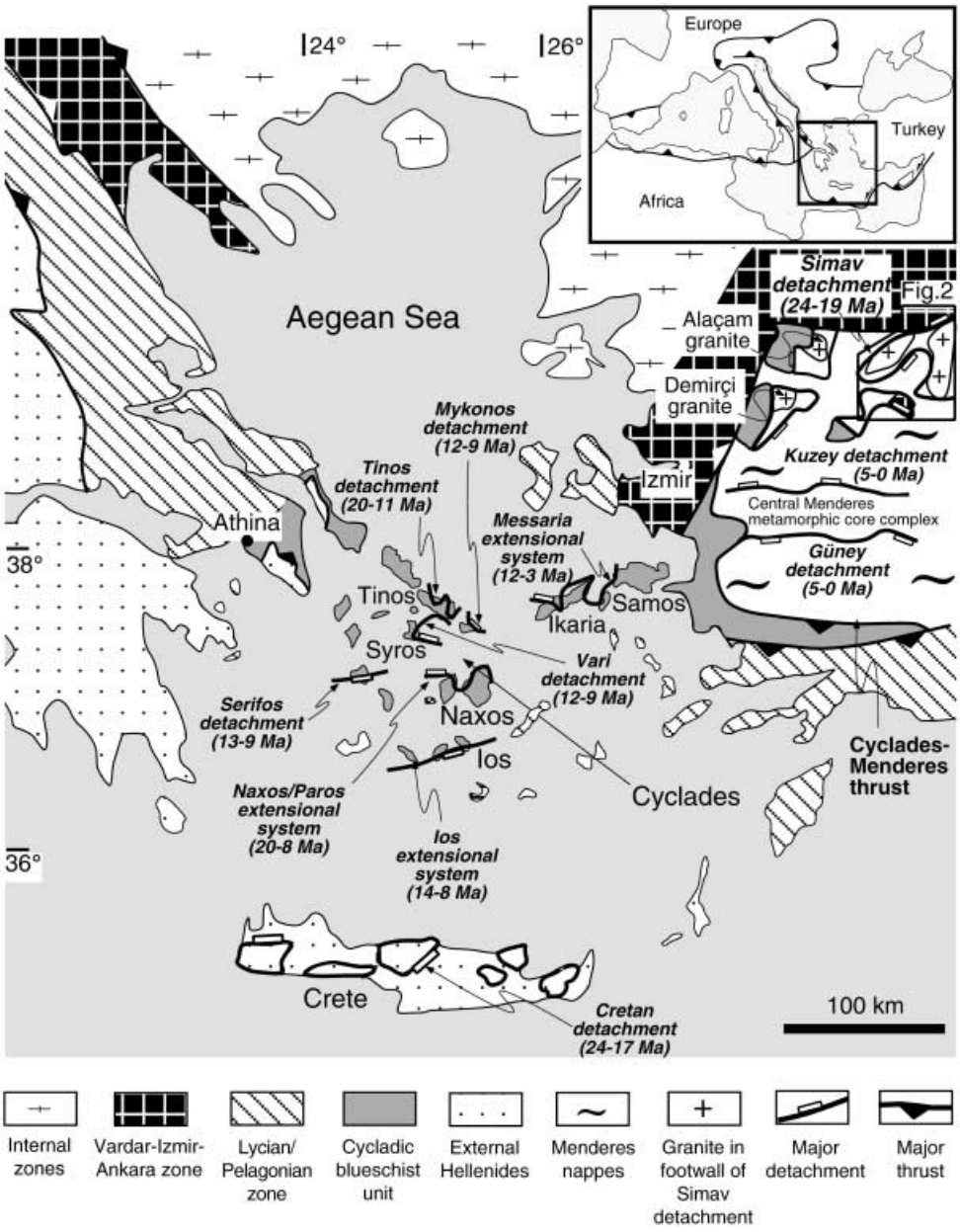

Fig. 1. Generalized tectonic map of the eastern Mediterranean showing major tectonic units and known extensional faults with approximate ages (data are from Lee & Lister 1992; John & Howard 1995; Thomson *et al*. 1999; Gessner *et al*. 2001*a*; Işik & Tekeli 2001; Ring *et al*. 1999*b*, 2003*b*; Kumerics *et al*. 2004); box indicates location of Figure 2. Movement on the Simav detachment stopped at *c*. 19 Ma, earlier than all other detachments in the region.

20–19 Ma (Gessner *et al*. 2001*a*; Ring *et al*. 2003*a*) and one single $^{40}Ar/^{39}Ar$ white mica age of 22.9 ± 0.5 Ma from a mylonite derived from Precambrian gneiss (Işik *et al*. 2004) suggest an age of *c*. 23–19 Ma for the Simav detachment.

The foliation in the footwall of the Simav detachment has a subhorizontal orientation and parallels the detachment fault. The foliation pattern in the rocks of the Vardar–İzmir–Ankara zone and the Cycladic blueschist unit in the hanging wall is less clear; however, it seems that the hanging wall is made up of a number of southward-tilted blocks. Neogene basin deposits north of Simav (Figs 2 and 3) dip *c*. 10–15° to the south. These rocks are cut by generally north-dipping normal faults. Ring *et al*. (2003*a*) estimated a dip angle of *c*. 15° for the Simav detachment and showed that the development of the detachment along the former thrust plane of the Cyclades–Menderes thrust controlled the low dip angle. The overall geometry across the Simav detachment resembles that across detachment faults in the nearby Aegean (Lister *et al*. 1984; Lee & Lister 1992; Ring *et al*. 2001, 2003*b*), which are also thought to have originated as low-angle detachment faults.

The Simav graben cuts the Simav detachment at a high angle (Fig. 3), is seismically active (Seyitoğlu 1997) and is associated with hydrothermal activity. The border fault of the asymmetric graben is located at its southern side and has created almost 1000 m of relief. Field relationships and the geomorphology associated with both faults show that the Simav graben is distinctly younger than the Simav detachment and that the structures are unrelated to each other.

In the centre of the Anatolide belt, a Pliocene to Recent phase of bivergent brittle detachment faulting is associated with the development of the Kuzey and Güney detachments and the still active Gediz and Büyük Menderes graben (Şengör 1987; Cohen *et al*. 1995; Seyitoğlu *et al*. 2000; Gessner *et al*. 2001*a*). The footwall of the top-to-the-north Kuzey detachment is a south-

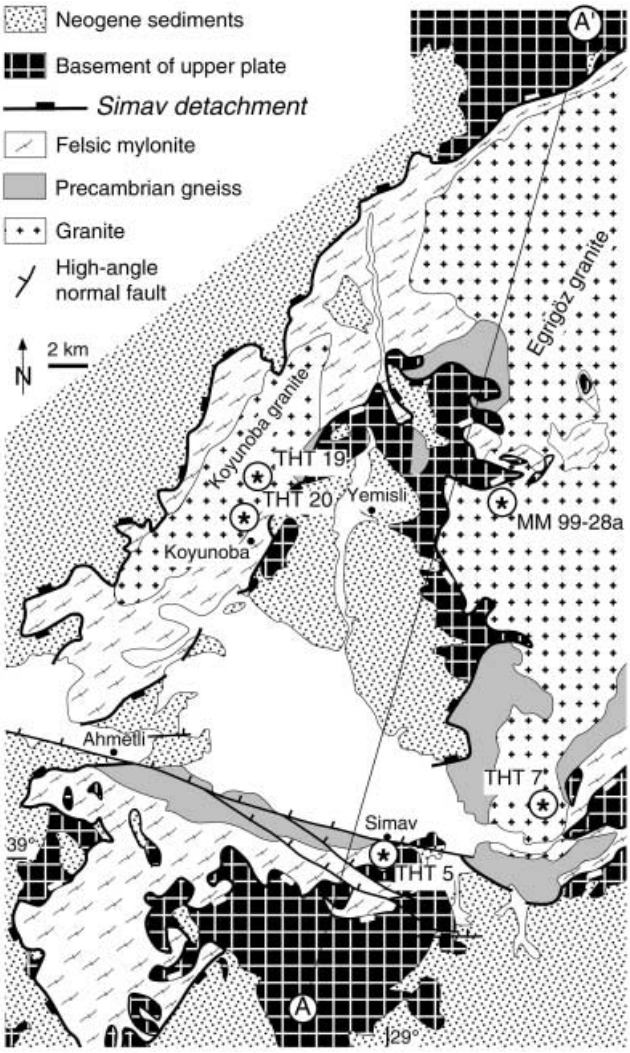

Fig. 2. Detailed map of the Simav metamorphic core complex and location of dated samples MM 99-28a and THT 7 from the Eğrigöz granite, samples THT 19 and 20 from the Koyunoba granite and sample THT 5 from a leucogranite dyke south of Simav. The basement of the upper plate includes rocks of the Vardar–İzmir–Ankara zone and of the Cycladic blueschist unit. The felsic mylonite is mainly mylonitized Eğrigöz and Koyunoba granite but, in part, also mylonitic Precambrian gneiss. Felsic mylonite makes up the base of Neogene sediments; line of cross-section A–A′ in Figure 3 is indicated.

ward-dipping monocline, whereas the footwall of the top-to-the-south Güney detachment is a northward-dipping monocline. Both monoclines combine to form a 50 km syncline that characterizes the structure of the Central Menderes metamorphic core complex (Gessner *et al*. 2001*a*) (Fig. 3), which is distinctly different from that of the Simav metamorphic core complex (Ring *et al*. 2003*a*).

Field relationships of granitoids and previous biotite dating

All granitoids in the footwall of the Simav detachment are dominated by medium- to coarse-grained granite, granodiorite, quartz monzonite, diorite and syenogranite. The Eğrigöz granite is strongly elongated in the NNE direction and is some 45 km by 10 km in plan section. Previous age dating yielded K–Ar biotite ages of 20.4 ± 0.6 Ma and 20.0 ± 0.7 Ma (Bingöl *et al*. 1982) and an $^{40}Ar/^{39}Ar$ biotite age of 20.2 ± 0.3 Ma (Işik *et al*. 2004). Four similar K–Ar biotite ages of 20.9 ± 0.5 Ma to 19.9 ± 0.7 Ma (with one exceptionally old age of 27.9 ± 1.9 Ma) and one white mica age of 18.6 ± 0.7 Ma were reported from the Alaçam granite further west (Bingöl *et al*. 1982). The Koyunoba granite is smaller in outcrop than the Eğrigöz granite but also strongly elongated in a NNE direction. The two granites are separated by felsic mylonite (Fig. 2), which progressively grades into undeformed Eğrigöz and Koyunoba granite and developed, at least in part, from those granites. Therefore, it is conceivable that both granites are a single large intrusion that was heterogeneously transformed into felsic mylonite at its top. The felsic mylonite makes up the base of the overlying Neogene sediments and therefore we propose, in line with Işik *et al*. (2004), that the sediments are allochthonous with respect to the granites. South of the Simav graben, the felsic mylonite is associated with a number of leucogranite dykes. A few of these dykes cut across a mylonitic fabric, whereas most dykes are strongly deformed with the felsic mylonite and show similar deformation structures. The leucogranite dykes also intrude into Precambrian gneiss (Fig. 4a and b).

SIMS U–Th–Pb zircon dating

Heavy minerals were separated from samples MM 99-28a and THT 7 of the Eğrigöz granite, samples THT 19 and 20 from the Koyunoba granite and sample THT 5 from a weakly deformed leucogranite dyke, which intrude into Precambrian gneiss (Figs 2 and 4b). Zircons were then hand picked, mounted, polished, cleaned and gold coated. Cathodoluminescence (CL) imaging was carried out to characterize the zircon and identify analysis spot sites. The zircons predominantly form elongate prisms with aspect ratios of >3:1. Under CL these crystals have irregularly zoned elongate cores and are surrounded by finely oscillatory zoned rims with common sector zonation (Figs 5–7). A couple of more equant grains were seen that in CL have sub-circular cores again rimmed with oscillatory zoned zircon (e.g. Fig. 5a).

U–Pb isotopic data were collected on a sensitive high-resolution ion microprobe (SHRIMP II), Perth, Australia. Sensitivity for Pb isotopes in zircon was *c*. 18 c.p.s. ppm^{-1} per nA, primary beam current was 2.5–3.0 nA, spot size was *c*. 25 μm diameter and mass resolution was *c*. 5000.

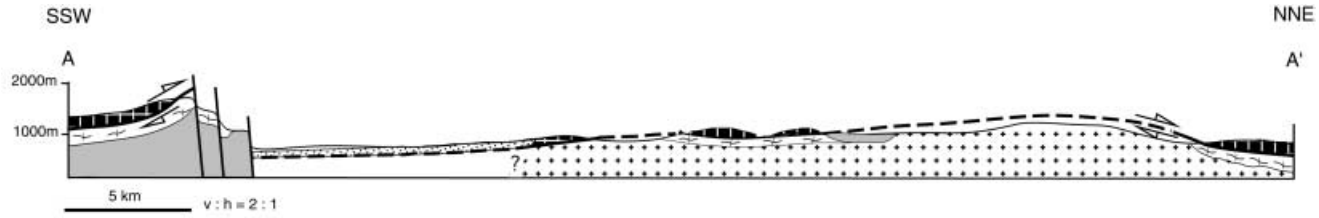

Fig. 3. Cross-section A–A′ showing the Eğrigöz granite in the footwall of Simav detachment. The southern limit of the granite is unknown. It should be noted that the vertical scale is twice the horizontal scale; symbols are the same as for Figure 2.

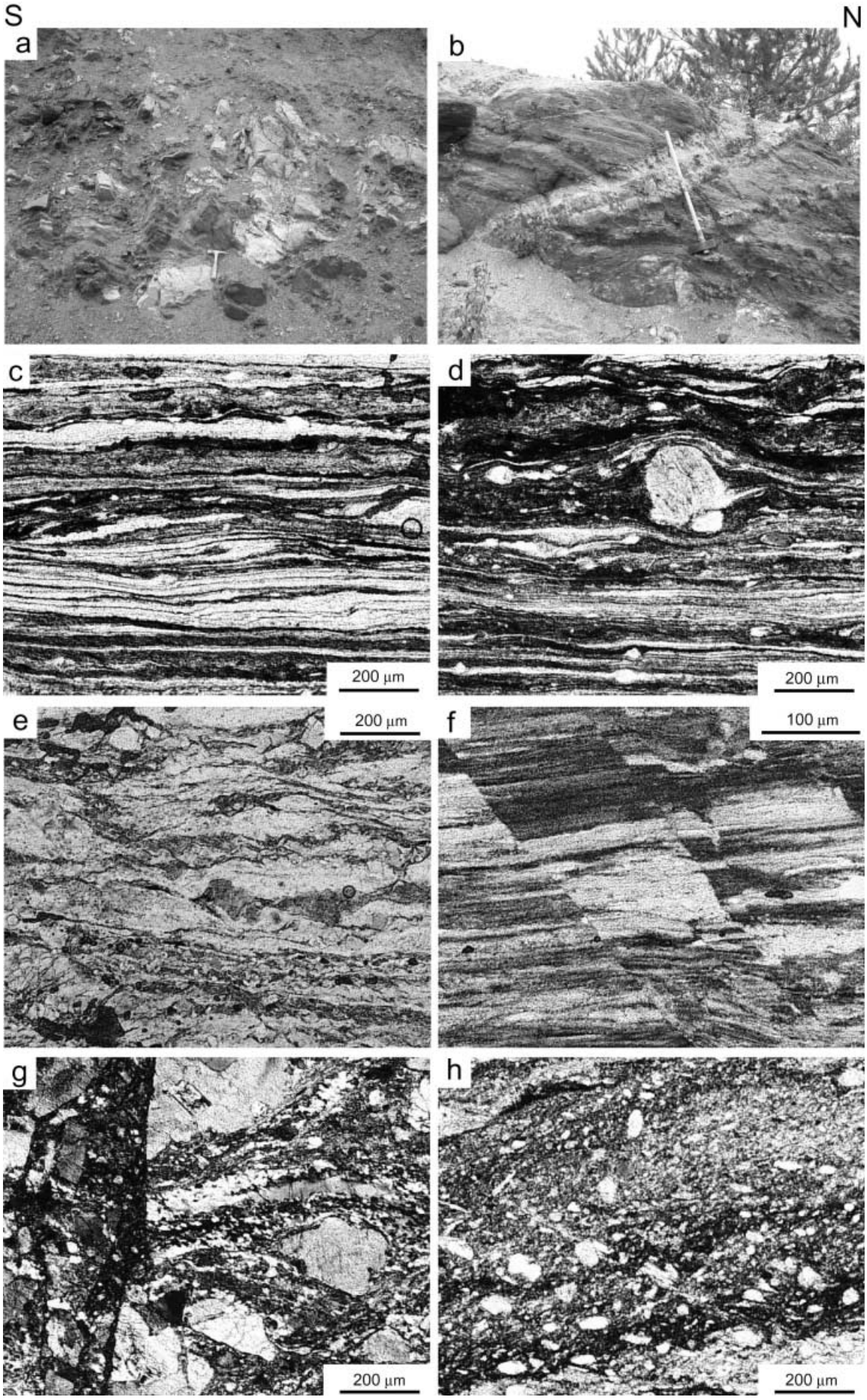
S
N
a
b
c
d
200 μm
200 μm
e
200 μm
f
100 μm
g
200 μm
h
200 μm

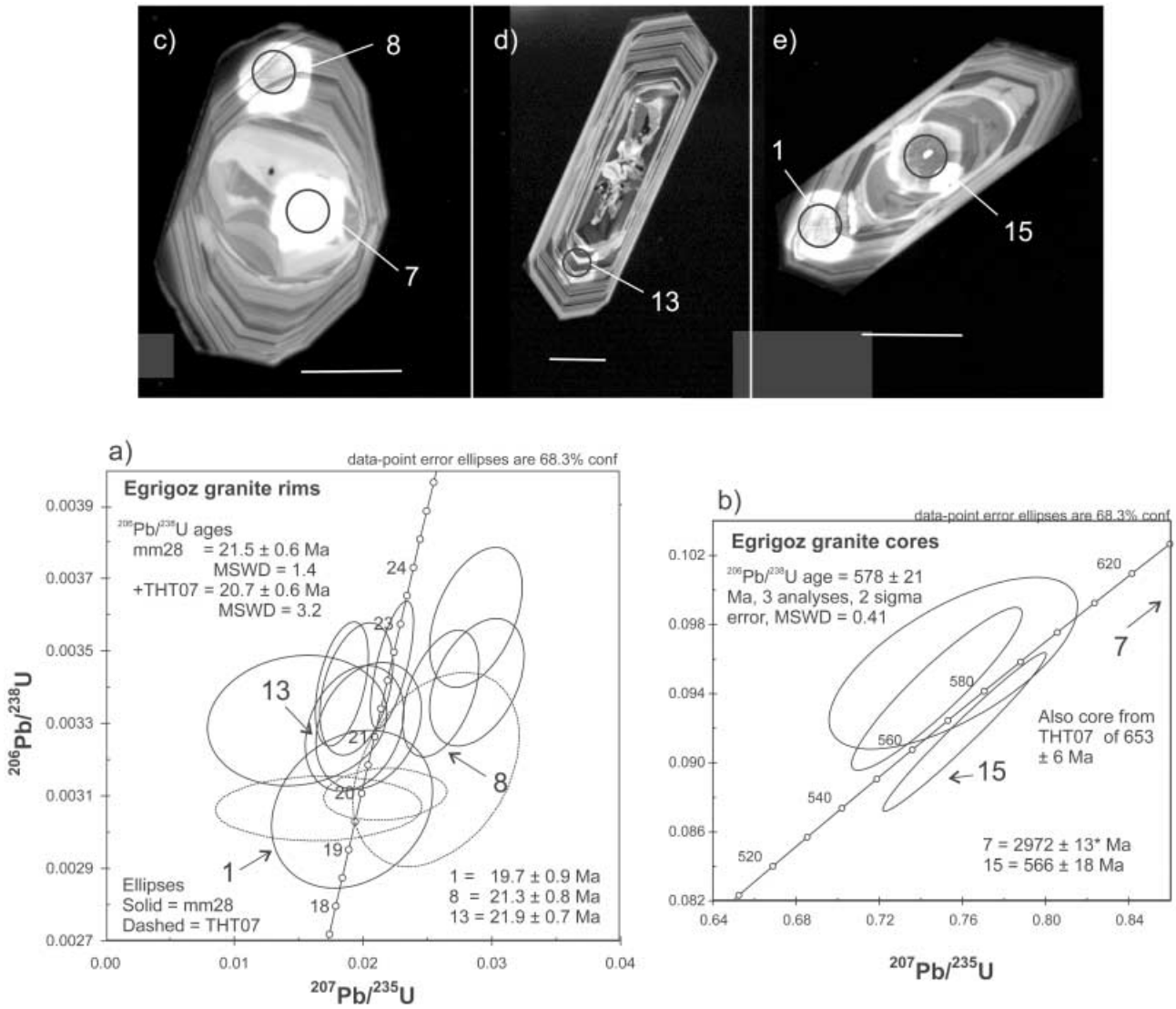

Fig. 5. Eğrigöz granite. (**a**) CL image of grain displaying irregularly zoned 2972 ± 13 Ma core rimmed with oscillatory-zoned 21.3 ± 0.8 Ma zircon. (**b**) Oscillatory zoned rim surrounding irregularly zoned core; rim age is 21.9 ± 0.7 Ma. (**c**) Irregularly zoned core dated at 566 ± 18 Ma and oscillatory zoned rim dated at 19.7 ± 0.9 Ma. Scale bar for all photographs represents 25 μm. (**d**) Concordia plot of oscillatory zoned magmatic rims from samples MM 99-28a and THT 7. (**e**) U–Pb concordia plot of Neoproterozoic cores. All quoted data-point ages refer to common Pb corrected $^{206}Pb/^{238}U$ ages except point 7 whose antiquity means that $^{207}Pb/^{206}Pb$ age (indicated by asterisk) is more precise. Errors for individual analyses are quoted at the 1σ level; weighted mean ages are quoted at the 2σ level.

Correction of measured isotopic ratios for common Pb was based on the measured ^{204}Pb in each sample and often represented a <1% correction to the ^{206}Pb counts (see % ^{206}Pbc in Table 1). Any common Pb component in the standard was interpreted as surface contaminant and modelled on the composition of Broken Hill ore Pb; additional common Pb in the unknowns was modelled on the approximate age of the grain using the Pb isotope evolution model of Stacey & Kramers (1975). Seven mass scans were undertaken on each analysis to enhance precision. Pb/U isotopic ratios were corrected for instrumental interelement discrimination using the observed covariation between Pb^+/U^+ and UO^+/U^+ (Hinthorne *et al*. 1979) determined from interspersed analyses of the Perth in-house standard zircon CZ3.

From sample MM 99-28a four cores were analysed; three were elongate, with a broadly elliptical form and yielded Neoproterozoic $^{206}Pb/^{238}U$ ages of 589 ± 19 Ma, 580 ± 18 Ma and 566 ± 18 Ma (Table 1) (note that errors for single analyses are quoted at the 1σ level; mean ages are quoted at 2σ). These are interpreted as xenocrystic cores and are of a similar age to zircon analysed elsewhere in the Anatolide belt of western Turkey (Loos & Reischmann 1999; Gessner *et al*. 2001*b*, 2004). The other core was concordant and produced a $^{207}Pb/^{206}Pb$ age of

Fig. 4. Field relationships of the leucogranite dykes: (**a**) irregular dykes cutting across pervasive foliation in mica schist; (**b**) a 30 cm wide dyke intruding into coarse-grained mica schist; the dyke cuts the penetrative foliation. Microstructures of the Eğrigöz granite: (**c**) quartz ribbons defining ultramylonitic foliation; (**d**) narrowly spaced foliation in quartz-rich layers in the lower part of microphotograph, asymmetric strain shadow around feldspar porphyroclast indicates top-to-the-NNE shear sense (note that feldspar has not recrystallized); (**e**) asymmetric fabrics around quartz and feldspar indicating top-to-the-NNE shear; (**f**) extremely narrow-spaced ultramylonitic foliation made up by quartz and sericite; feldspar is completely transformed to sericite; microfaults indicate top-to-the-NNE normal faulting; (**g**) breccia zone cutting at high angle across ductile foliation; (**h**) cataclastically reworked foliation.

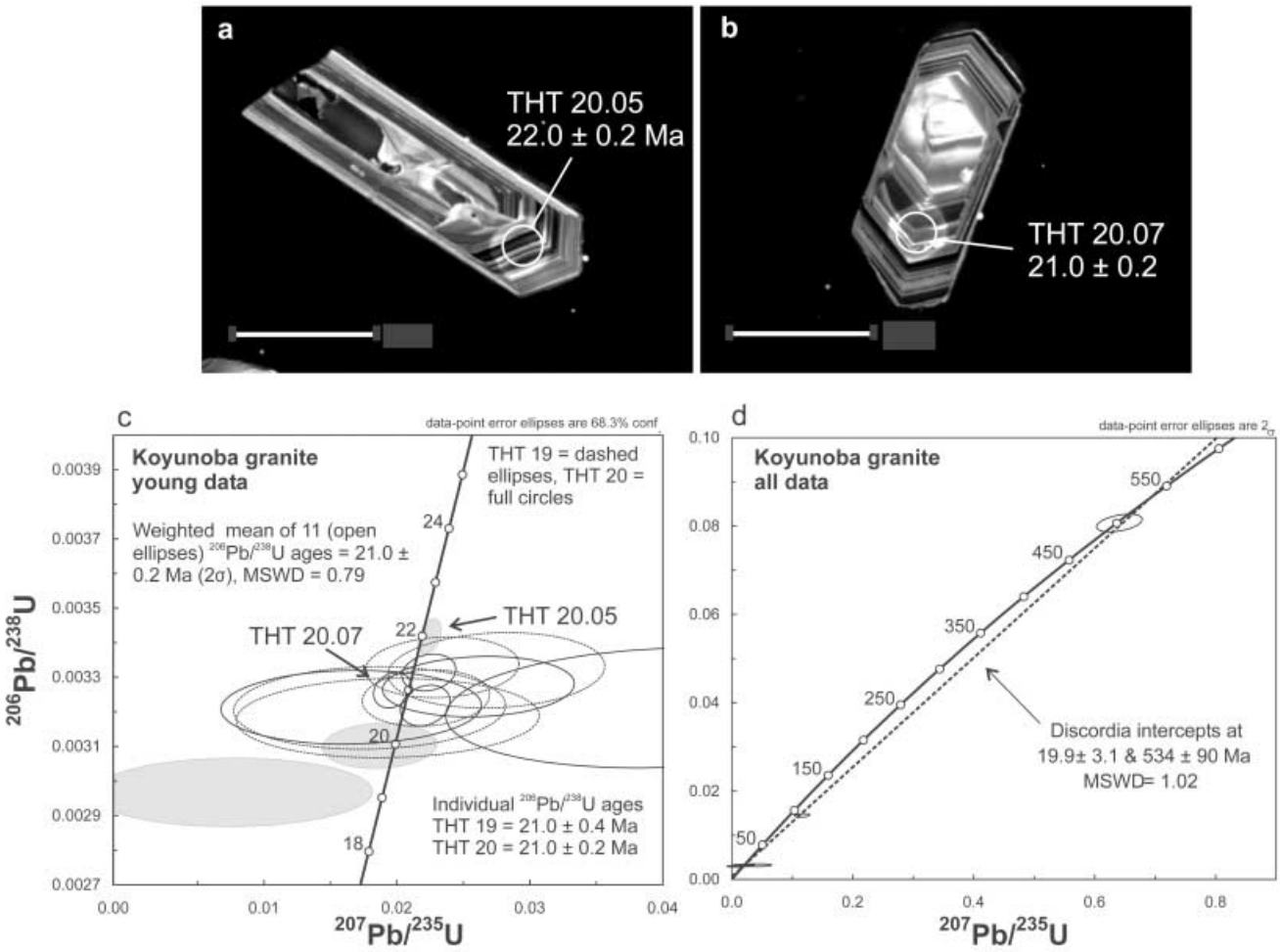

Fig. 6. Koyunoba granite. (**a**) Pristine oscillatory zoned rim surrounding irregularly zoned core of long-prismatic zircon. (**b**) CL image of grain displaying core rimmed with oscillatory zoned zircon. Scale bar for both photographs represents 100 μm. (**c**) U–Pb concordia plot of oscillatory zoned magmatic rims yielding mean age of 21.0 ± 0.2 Ma for Koyunoba granite. Grey filled ellipses represent analyses of THT 20 not used in calculating the mean age. (**d**) Concordia diagram showing discordia line constructed from dated zircon from the Koyunoba granite, samples THT 19 and THT 20. All quoted data-point ages refer to common Pb corrected $^{206}Pb/^{238}U$ ages. Errors for individual analyses are quoted at the 1σ level; weighted mean ages are quoted at the 2σ level.

2972 ± 13 Ma (the $^{207}Pb/^{206}Pb$ age is quoted because at this antiquity it is more precise than the $^{206}Pb/^{238}U$ age). All cores are rimmed with new zircon growth that has a mean $^{206}Pb/^{238}U$ age of 21.5 ± 0.7 Ma (Fig. 5d). In fact, the impressive age range of *c*. 2950 Ma between core and rim in one grain (spots 7 and 8, Fig. 5a) is the largest age range we know of yet analysed in a single grain. The zircon rims of sample THT 7 from the southern part of the pluton yielded similar results. One analysed core yielded a Neoproterozoic $^{206}Pb/^{238}U$ age of 653 ± 6 Ma (Table 1). The cores were rimmed with new zircon growths with $^{206}Pb/^{238}U$ ages ranging from 20.3 ± 1.1 Ma to 19.6 ± 0.3 Ma (Table 1). The oscillatory zoned nature of all analysed rims from samples MM 99-28a and THT 7 indicates that the zircon crystallized from a melt; the mean age from both samples of 20.7 ± 0.6 Ma (MSWD = 3.2) is therefore interpreted as the crystallization age of the synkinematic Eğrigöz granite.

Two cores were analysed from sample THT 20 from the Koyunoba granite. These yielded a Cambrian $^{206}Pb/^{238}U$ age of 500 ± 5 Ma and, surprisingly, a Cretaceous $^{206}Pb/^{238}U$ age of 93 ± 1 Ma (Table 1). This latter zircon has an Early Cambrian $^{207}Pb/^{206}Pb$ age of 540 ± 96 Ma and lies on a discordia line tying the other Cambrian core age with the age of the rims (Fig. 6d), suggesting that it is discordant and either partially lost Pb or the analysis spot sampled zircon of two generations. These cores are interpreted as xenocrysts. Zircon from sample THT 19 are similar to those in THT 20. In both samples, cores are rimmed by new zircon growth that has a mean $^{206}Pb/^{238}U$ age of 21.0 ± 0.2 Ma (MSWD = 0.79) (Fig. 6c), which we interpret as the crystallization age of the synkinematic Koyunoba granite. This intrusion age is within error of the mean age of 20.7 ± 0.6 Ma obtained for the Eğrigöz granite.

The leucogranite dyke THT 5 yielded similar results. There are many xenocrystic cores that have $^{206}Pb/^{238}U$ ages ranging from 640 ± 7 Ma to 511 ± 6 Ma. One zircon core yielded a Triassic $^{206}Pb/^{238}U$ age of 257 ± 3 Ma. This analysis is highly discordant and does not necessarily indicate zircon formation in the Triassic. It is more likely that this zircon formed earlier and lost Pb in the Tertiary to produce this mixed age. The newly crystallized zircon rims give a mean $^{206}Pb/^{238}U$ age of 24.4 ± 0.3 Ma with two older zircon cores and rims of *c*. 28 Ma (Fig. 7).

Synkinematic emplacement of the dated granites

Large parts of the Eğrigöz and Koyunoba granites are undeformed and exhibit magmatic textures. Aligned igneous minerals of euhedral potassium feldspar, plagioclase, biotite and hornblende in an undeformed quartz matrix define a magmatic foliation. Microgranitic enclaves, xenoliths and schlieren layering are oriented parallel to this foliation. Petrography shows that the minerals in the enclaves, those in the schlieren layering, and also

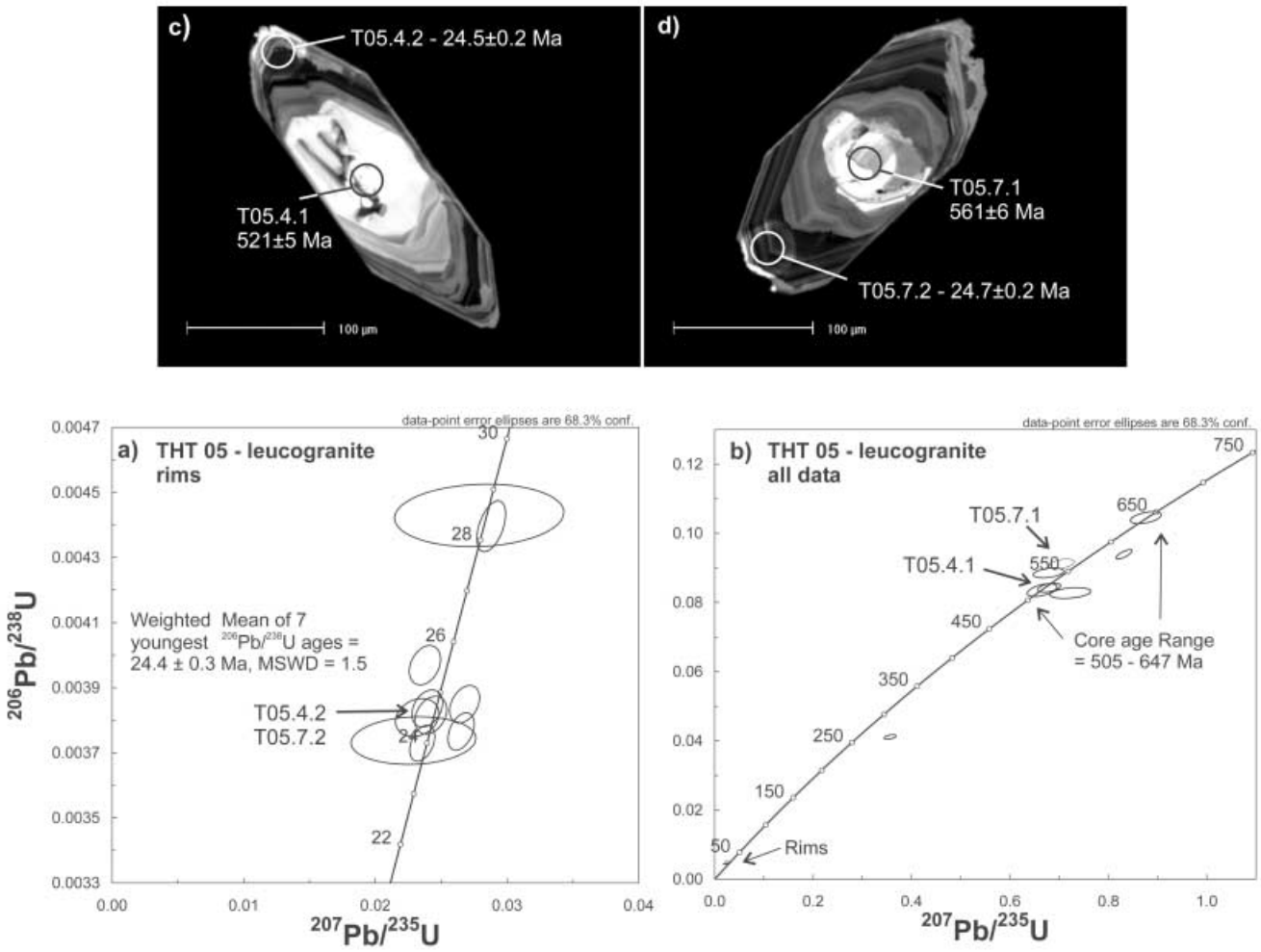

Fig. 7. Leucogranite dyke. (**a**) Oscillatory zoned rim surrounding irregular Cambrian core. (**b**) CL image of grain displaying irregularly zoned core rimmed with oscillatory zoned zircon. Scale bar for both photographs represents 100 µm. (**c**) U–Pb concordia plot of oscillatory zoned magmatic rims. (**d**) U–Pb concordia diagram data from all dated zircon from the leucogranite dyke, sample THT 5. All quoted data-point ages refer to common Pb corrected $^{206}Pb/^{238}U$ ages. Errors for individual analyses are quoted at the 1σ level; weighted mean ages are quoted at the 2σ level.

those forming the magmatic foliation do not show any signs of deformation or recrystallization. In the upper parts of both granites, the magmatic foliation lies in a subhorizontal orientation. Here a weak NNE-trending magmatic lineation is defined by preferred orientation of the long axes of prismatic potassium feldspar.

In their uppermost parts the Eğrigöz and Koyunoba granites are progressively deformed into mylonite with a subhorizontal tectonic foliation associated with a NNE-trending stretching lineation. The mylonitic foliation is defined by medium- to fine-grained flattened and strongly elongated quartz grains and aligned mica (Fig. 4c–f). The foliation may be spaced at the millimetre scale or is extremely narrowly spaced at the micro-millimetre scale (Fig. 4f). The lineation is expressed by stretched quartz, smeared-out mica and recrystallized quartz tails on feldspar porphyroclasts. Quartz commonly forms polycrystalline ribbons (Fig. 4c and d) and shows undulatory extinction, dynamic recrystallization and grain-boundary migration. Micas are commonly recrystallized into small new grains, which define C-planes that lie at a small angle to the mylonitic foliation. The ductile structures show a progressive evolution into semi-ductile and brittle deformation. Throughout the upper parts of the Eğrigöz and Koyunoba granites, potassium feldspar porphyroclasts and hornblende show brittle micro-normal faults at moderate to high angles to the mylonitic foliation. These microfaults are commonly pulled apart with growth of new quartz and biotite between pulled apart feldspar and hornblende. About 30–50 m beneath the detachment fault, granite mylonite is brecciated and fractured and forms cataclasite and ultracataclasite (Fig. 4g and h); occasionally pseudotachylite occurs. Very fine-grained retrograde chlorite is common in the breccia zones and feldspar is severely altered to sericite.

At the meso- and microscale, shear bands, S–C fabrics, oblique quartz grain-shape foliations, asymmetric biotite fish, asymmetric strain shadows around feldspar porphyroclasts (Fig. 4) and Riedel structures indicate a consistent top-to-the-NNE shear sense (see also Işik & Tekeli 2001; Işik *et al*. 2004).

The leucogranite dykes and the felsic mylonite have a subhorizontal foliation associated with a NNE-trending stretching lineation. The foliation is defined by flattened and strongly elongated quartz. The lineation is expressed by stretched quartz aggregates. Feldspar porphyroclasts are not plastically deformed

Table 1. *U–Th–Pb isotopic data and calculated ages from SIMS zircon analyses using the SHRIMP II from the Eğrigöz (MM 99-28a, THT 7) and Koyunoba (THT 20 and THT 19) granites and leucogranite (THT 5)*

Analyses	Type	Conc. (ppm)		$^{232}Th/^{238}U$	% ^{206}Pbc	Isotopic ratios						Ages (Ma)						% discor.
		U	Th			$^{206}Pb^{1}/^{238}U$	±2	$^{207}Pb^{1}/^{235}U$	±	$^{207}Pb^{1}/^{206}Pb$	±	$^{206}Pb^{1}/^{238}U$	±	$^{208}Pb^{1}/^{232}Th$	±	$^{207}Pb^{1}/^{206}Pb$	±	
MM 28.01	R	803	211	0.27	0.64	0.0031	0.0001	0.0191	0.0041	0.0454	0.0095	20.0	0.8	19.3	5.7	−35	510	−274
MM 28.02	R	789	177	0.23	0.80	0.0034	0.0001	0.0195	0.0019	0.0416	0.0037	21.4	0.5	17.8	2.6	−250	226	−1267
MM 28.03	R	812	263	0.33	0.77	0.0033	0.0001	0.0193	0.0025	0.0426	0.0054	20.5	0.5	19.4	2.7	−189	317	−1023
MM 28.04	R	789	269	0.35	0.70	0.0033	0.0001	0.0204	0.0027	0.0450	0.0058	20.3	0.5	20.5	2.7	−58	313	−385
MM 28.05	R	996	476	0.49	−1.03	0.0036	0.0001	0.0288	0.0024	0.0581	0.0043	22.5	0.5	27.1	2.0	532	163	2263
MM 28.06	R	1050	379	0.37	−1.04	0.0034	0.0001	0.0260	0.0020	0.0558	0.0037	20.7	0.4	25.3	1.8	446	149	2050
MM 28.07	C	82	90	1.14	0.00	0.6003	0.0206	18.1154	0.6391	0.2189	0.0018	2949	55	2900	73	2972	13	1
MM 28.08	R	990	400	0.42	1.76	0.0033	0.0001	0.0148	0.0046	0.0326	0.0100	20.6	0.5	16.8	3.9	−913	895	−4529
MM 28.09	C	100	67	0.69	0.52	0.0957	0.0033	0.7557	0.0393	0.0573	0.0022	586	13	579	20	502	86	−14
MM 28.10	R	1708	1182	0.72	−1.57	0.0034	0.0001	0.0288	0.0024	0.0613	0.0047	21.7	0.5	25.1	1.3	648	164	2889
MM 28.11	C	608	31	0.05	0.14	0.0942	0.0031	0.7478	0.0269	0.0576	0.0008	565	11	499	42	514	30	−9
MM 28.12	R	3776	1675	0.46	0.04	0.0035	0.0001	0.0222	0.0011	0.0466	0.0017	22.1	0.5	22.2	0.8	27	88	23
MM 28.13	R	3605	3333	0.96	0.98	0.0034	0.0001	0.0183	0.0014	0.0390	0.0026	20.6	0.4	19.2	0.6	−417	172	−2127
MM 28.14	R	716	307	0.44	7.11	0.0031	0.0001				0.0000	19.7	0.6	5.1	6.1			
MM 28.15	C	622	585	0.97	−0.01	0.0917	0.0030	0.7611	0.0259	0.0602	0.0004	554	10	567	11	611	15	10
THT 7.02.1	C	489	91	0.19	0.14	0.1066	0.0011	0.9226	0.0135	0.0628	0.0007	653	6	663	11	701	23	7
THT 7.02.2	R	541	83	0.16	3.38	0.0030	0.0001	0.0165	0.0053	0.0394	0.0126	19.6	0.4	12.4	11.3	−391	832	−2096
THT 7.03.1	R	674	185	0.28	1.79	0.0031	0.0000	0.0217	0.0032	0.0510	0.0074	19.9	0.3	24.7	3.8	242	333	1119
THT 7.03.2	R	844	369	0.45	0.32	0.0032	0.0002	0.0256	0.0043	0.0589	0.0092	20.3	1.1	26.6	3.9	564	341	2675
THT 20.03	R	741	886	1.24	1.41	0.0033	0.0001	0.0261	0.0047	0.0579	0.0105	21.0	0.4	22.2	1.5	525	396	2393
THT 20.04	R	572	263	0.48	7.34	0.0030	0.0001	0.0076	0.0069	0.0187	0.0170	19.1	0.4	9.1	4.8	−2950	4328	−15566
THT 20.05	R	7940	1338	0.17	0.20	0.0034	0.0000	0.0224	0.0006	0.0476	0.0011	22.0	0.2	23.9	0.9	78	56	254
THT 20.06	C	421	21	0.05	0.23	0.0807	0.0008	0.6409	0.0155	0.0576	0.0013	500	5	590	74	515	48	3
THT 20.07	R	3466	805	0.24	0.58	0.0033	0.0000	0.0197	0.0009	0.0437	0.0021	21.0	0.2	20.9	1.3	−126	116	−702
THT 20.08	R	4110	404	0.10	0.22	0.0033	0.0000	0.0224	0.0013	0.0490	0.0029	21.3	0.2	22.2	4.6	150	137	602
THT 20.09	R	1042	300	0.30	2.04	0.0031	0.0000	0.0187	0.0028	0.0437	0.0066	19.9	0.3	20.2	3.3	−126	372	−733
THT 20.10	R	491	213	0.45	3.49	0.0032	0.0001	0.0165	0.0064	0.0374	0.0145	20.7	0.5	18.7	5.2	−529	1041	−2659
THT 20.11	R	226	91	0.42	1.53	0.0032	0.0001	0.0400	0.0108	0.0904	0.0242	20.6	0.7	38.4	10.3	1434	511	6847
THT 20.12	C	790	258	0.34	0.37	0.0145	0.0002	0.1164	0.0052	0.0583	0.0026	92.7	1.0	44.1	4.5	540	96	483
THT 20.13	R	1925	1746	0.94	0.36	0.0032	0.0000	0.0221	0.0012	0.0499	0.0027	20.7	0.3	21.4	0.6	188	127	810
THT 19.1.1	C	805.8499826	710.1240568	0.910526654	3.948664799	0.0032	0.0001	0.0192	0.0072	0.0441	0.0165	20.4	0.4	19.4	2.9	−104	922	−610
THT 19.2.1	R	705.6354595	201.517671	0.295083807	3.65458705	0.0032	0.0001	0.0178	0.0065	0.0406	0.0147	20.5	0.5	15.9	7.9	−313	926	−1626
THT 19.3.1	R	1301.902922	520.0188603	0.412717736	1.313586619	0.0033	0.0001	0.0233	0.0037	0.0510	0.0081	21.3	0.3	22.0	3.5	241	366	1032
THT 19.4.1	R	1332.202011	255.9286261	0.198500415	1.597175814	0.0033	0.0000	0.0223	0.0031	0.0497	0.0068	20.9	0.3	22.2	4.5	181	319	763
THT 19.5.1	R	733.1385796	381.5368476	0.537728497	1.846838506	0.0033	0.0001	0.0276	0.0053	0.0601	0.0115	21.4	0.4	24.6	3.8	607	413	2734
THT 5.01.1	C	89	39	0.45	0.22	0.0825	0.0010	0.7224	0.0274	0.0635	0.0023	511	6	562	19	725	76	42
THT 5.01.2	R	4132	171	0.04	0.13	0.0038	0.0000	0.0267	0.0007	0.0504	0.0013	24.7	0.2	30.9	4.1	215	61	769
THT 5.02.1	C	663	8	0.01	1.45	0.0044	0.0001	0.0278	0.0042	0.0456	0.0069	28.5	0.4			−25	365	−188
THT 5.02.2	R	3109	61	0.02	−0.02	0.0038	0.0000	0.0265	0.0007	0.0510	0.0012	24.2	0.2	61.5	6.0	243	53	903
THT 5.03.1	C	1086	241	0.23	0.09	0.0938	0.0009	0.8320	0.0104	0.0643	0.0005	578	5	761	10	752	17	30
THT 5.03.2	R	6402	31	0.01	0.26	0.0037	0.0000	0.0235	0.0006	0.0458	0.0011	24.0	0.2	22.4	29.4	−12	58	−149
THT 5.04.1	C	298	47	0.16	0.22	0.0841	0.0009	0.6796	0.0155	0.0586	0.0012	521	5	445	24	552	44	6
THT 5.04.2	R	4033	51	0.01	0.75	0.0038	0.0000	0.0232	0.0011	0.0442	0.0020	24.5	0.2			−102	113	−517
THT 5.05.1	C	480	70	0.15	0.24	0.0407	0.0004	0.3572	0.0082	0.0636	0.0013	257	3	372	13	730	43	184
THT 5.05.2	R	3890	146	0.04	0.16	0.0038	0.0000	0.0242	0.0008	0.0460	0.0015	24.5	0.2	28.3	5.7	−3	77	−112
THT 5.06.1	C	243	201	0.86	0.29	0.1044	0.0012	0.8754	0.0208	0.0608	0.0013	640	7	650	10	632	45	−1
THT 5.06.2	R	1390	20	0.01	1.59	0.0037	0.0000	0.0229	0.0031	0.0444	0.0060	24.0	0.3			−87	331	−462
THT 5.07.1	C	269	32	0.12	0.29	0.0909	0.0010	0.7049	0.0171	0.0562	0.0012	561	6	616	35	461	49	−18
THT 5.07.2	R	5499	278	0.05	0.31	0.0038	0.0000	0.0239	0.0008	0.0452	0.0014	24.7	0.2	22.6	3.7	−43	73	−273
THT 5.08.1	C	235	30	0.13	0.40	0.0884	0.0009	0.6780	0.0205	0.0556	0.0016	546	6	485	43	437	63	−20
THT 5.08.2	R	5742	79	0.01	0.43	0.0040	0.0000	0.0237	0.0008	0.0434	0.0014	25.5	0.3			−143	78	−662
THT 5.09.1	C	318	18	0.06	0.30	0.0834	0.0012	0.6652	0.0199	0.0578	0.0015	517	7	492	74	523	57	1
THT 5.09.2	R	7092	53	0.01	0.25	0.0044	0.0001	0.0287	0.0007	0.0474	0.0010	28.3	0.3	30.8	22.0	72	51	153

The apparent discordance of *c*. 20 Ma grains is probably an artefact of the common Pb correction as small errors in correction for young ages give large concordance errors at young ages; common Pb derived from measured ^{204}Pb assuming Broken Hill Pb isotopic ratio; data processed using programs SQUID and ISOPLOT. % ^{206}Pbc is percentage of common ^{206}Pb; R, rim; C, core analysis. All errors are absolute, 1σ errors.
aRadiogenic Pb only.

and are strongly transformed into sericite in high-strain zones. Quartz commonly forms polycrystalline ribbons; undulatory extinction, dynamic recrystallization and grain-boundary migration are widespread. It is conceivable that there are many more leucogranitic dykes, which because of mylonitic deformation are indistinguishable from the felsic mylonite. South of Simav, weakly deformed leucogranite dykes intrude into Precambrian gneiss (Fig. 4a and b) and cut across a penetrative foliation.

The parallelism between magmatic and mylonite foliations in the upper parts of the Eğrigöz and Koyunoba granites beneath the Simav detachment, and the progressive increase in first a suprasolidus crystal alignment and then a subsolidus mineral-deformation fabric as the Simav detachment is approached, is used to indicate the syndetachment intrusion of the Eğrigöz and Koyunoba granites. We cannot prove that the leucogranite dykes are synkinematic with respect to the Simav detachment. However, because some dykes cut across a mylonitic fabric whereas others are mylonitically deformed we infer synkinematic emplacement of the dykes.

Implications and conclusions

The structural development of the Eğrigöz and Koyunoba granites and the parallelism of magmatic and tectonic structures in their upper parts indicate that both granites intruded synkinematically at 21.3–20.1 Ma (at maximum 2σ uncertainty) into the footwall of the Simav detachment. The leucogranite dyke sampled further south intruded earlier at 24.4 ± 0.3 Ma, probably also synkinematically to the Simav detachment. The almost concordant U–Th–Pb zircon (21.3–20.1 Ma) and K–Ar and $^{40}Ar/^{39}Ar$ biotite ages of 21.0–19.3 Ma (at 2σ uncertainty) (Bingöl *et al*. 1982; Işik *et al*. 2004) from the Eğrigöz and Koyunoba granites, the leucogranite age of 24.4 ± 0.3 Ma, the mylonitization age of 22.9 ± 0.5 Ma (Işik *et al*. 2004) and the apatite fission-track ages (20–19 Ma; Gessner *et al*. 2001*a*; Ring *et al*. 2003*a*) from Precambrian gneiss suggest that the Simav detachment operated over a short time period between 24 and 19 Ma.

The intrusion age of the Eğrigöz granite (20.7 ± 0.6 Ma) is within error of the K–Ar and $^{40}Ar/^{39}Ar$ biotite ages (21.0–19.3 Ma). The data indicate very rapid cooling of the order of $>200\ ^{\circ}C\ Ma^{-1}$ for the granite during and after synkinematic emplacement and most probably indicate a very shallow intrusion depth. We speculate that very rapid cooling also characterizes the other synkinematic granites in the footwall of the Simav detachment (Fig. 1). The fact that feldspar in the granites did not deform ductilely also suggests very rapid cooling from *c*. 700 °C to *c*. 450 °C and high strain rates. Apatite fission-track data from Precambrian gneiss of the footwall of the Simav detachment south of Simav give Early Miocene cooling rates of $<100\ ^{\circ}C\ Ma^{-1}$ (Gessner *et al*. 2001*a*; Ring *et al*. 2003*a*). The slower cooling rates in the gneiss reflect the high-level intrusion of the Eğrigöz and Koyunoba granites and that the gneiss was much colder during detachment faulting than the synkinematic granites and had less potential for rapid cooling. Detachment-related deformation in the surrounding mylonitic gneiss includes quartz recrystallization and widespread brittle faulting. In the hanging-wall rocks, detachment-related deformation was entirely brittle. Overall, the deformation features suggest that the detachment was rooted in a relatively high crustal position, most probably at the brittle–ductile transition and that footwall rocks were exhumed from the uppermost ductile crust. This is corroborated by the general lack of feldspar ductility. In extensional settings associated with large granite intrusion, the geothermal field gradient is usually of the order of $>30\ ^{\circ}C\ km^{-1}$ (Hill *et al*. 1992; Kumerics *et al*. 2004) and therefore feldspar behaves ductilely at depths of *c*. 15 km.

It is interesting to note that the large Eğrigöz and Koyunoba granites are the northernmost exposed footwall rocks below the top-to-the-NNE Simav detachment. We hypothesize that the intrusion of these two large granites changed the stress geometry and rheology in such a way that no additional footwall material was dragged to the surface beneath the Simav detachment. Because displacement on the Simav detachment is at least 50 km (Işik *et al*. 2003; Ring *et al*. 2003*a*), this conclusion would indicate that the granites intruded late during detachment faulting and/or slip was very fast.

The Late Oligocene to Early Miocene age of the Simav detachment is about 20–15 Ma older than the still active Kuzey and Güney detachments in the central Anatolide belt and the also active Simav graben. The Salihli granodiorite in the footwall of the Kuzey detachment is of similar age to the Eğrigöz and Koyunoba granites but cooled significantly more slowly than the latter (Ring *et al*. 2003*a*). Gessner *et al*. (2001*a*) and Seyitoğlu *et al*. (2002) showed that the Kuzey and Güney detachments originated as high-angle faults that were rotated into a subhorizontal position and were then cut by high-angle normal faults that bound the Gediz and Büyük Menderes graben above both detachments. This rotation caused the large-scale monoclines that characterize the footwall geometry of the Güney and Kuzey detachments. The geometry of the Simav detachment is distinctly different and activity on the detachment in the Late Oligocene and Early Miocene was not associated with the development of a discrete graben in the hanging wall and of a large-scale monocline in the footwall. This, and the shallow dip of the Neogene sediments above the detachment, suggests that the Simav detachment originated in a low-angle position. The Simav graben above the Simav detachment can be linked with Pliocene to Recent extensional deformation in western Turkey. Although this latest phase of extension is mainly concentrated in the central Anatolide belt, the Simav graben implies that Pliocene–Recent extension also affected the northern Anatolide belt and that there are two superimposed extensional events in the Simav region.

This study was funded by Deutsche Forschungsgemeinschaft (grant Ri 538/15) and the Australian Research Council. We thank K. Gessner for discussions, V. Işik for sending the unpublished Tekeli *et al*. abstract and a preprint of the Işik *et al*. (2004) paper, and S. Thomson for providing zircons from the THT samples. SHRIMP II is operated by consortium consisting of Curtin University of Technology, the Geological Survey of Western Australia, and The University of Western Australia with support from the Australian Research Council. We appreciate the assistance of P. Kinny, S. Nemchin and A. Kennedy during SHRIMP analysis and data reduction. K. Ludwig is thanked for providing his data reduction and plotting programs SQUID and ISOPLOT 2.49. A.S.C.'s contribution forms Tectonics Special Research Centre Publication 300. We thank P. Hoskin and M. Whitehouse for helpful reviews.

References

Bingöl, E., Delaloye, M. & Ataman, G. 1982. Granitic intrusions in western Anatolia: a contribution to the geodynamic study of this area. *Eclogae Geologicae Helvetiae*, **75**, 437–446.

Bozkurt, E. 2000. Timing of extension on the Büyük Menderes Graben, western Turkey, and its tectonic implications. *In:* Bozkurt, E., Winchester, J.A. & Piper, J.D.A. (eds) *Tectonics and Magmatism in Turkey and Surrounding Regions*. Geological Society, London, Special Publications, **173**, 385–403.

Candan, O., Dora, Ö.O., Oberhänsli, R., Oelsner, F. & Dürr, S. 1997. Blueschist relics in the Mesozoic cover series of the Menderes Massif and correlations with Samos Island, Cyclades. *Schweizerische Mineralogische und*

Petrographische Mitteilungen, **77**, 95–99.

Cohen, H.A., Dart, C.J., Akyüz, H.S. & Barka, A. 1995. Syn-rift sedimentation and structural development of Gediz and Büyük Menderes grabens, western Turkey. *Journal of the Geological Society, London*, **152**, 629–638.

Collins, A.S. & Robertson, A.H.F. 1997. Lycian melange, southwestern Turkey: an emplaced Late Cretaceous accretionary complex. *Geology*, **25**, 255–258.

Collins, A.S. & Robertson, A.H.F. 1998. Processes of Late Cretaceous to Late Miocene episodic thrust-sheet translation in the Lycian Taurides, SW Turkey. *Journal of the Geological Society, London*, **155**, 759–772.

Coney, P.J. 1980. Cordilleran metamorphic core complexes; an overview. *In:* Crittenden, M.D.J., Coney, P.J. & Davis, G.H. (eds) *Cordilleran Metamorphic Core Complexes*. Geological Society of America, Memoirs, **xx**, 7–31.

Gans, P.B., Mahood, G.A. & Schermer, E.R. 1989. Synextensional magmatism in the Basin and Range province; a case study from the eastern Great Basin. *Geological Society of America, Special Papers*, **233**, 1–53.

Gessner, K., Ring, U., Johnson, C., Hetzel, R., Passchier, C. & Güngör, T. 2001a. An active bivergent rolling-hinge detachment system: the Central Menderes metamorphic core complex in western Turkey. *Geology*, **29**, 611–614.

Gessner, K., Piazolo, S., Güngör, T., Ring, U., Kröner, A. & Passchier, C.W. 2001b. Tectonic significance of deformation patterns in granitoid rocks of the Menderes nappes, Anatolide belt, southwest Turkey. *International Journal of Earth Sciences*, **89**, 766–780.

Gessner, K., Ring, U., Passchier, C.W. & Güngör, T. 2001c. How to resist subduction: evidence for large-scale out-of-sequence thrusting during Eocene collision in western Turkey. *Journal of the Geological Society, London*, **158**, 769–784.

Gessner, K., Collins, A.S., Ring, U. & Güngör, T. 2004. Structural and thermal history of poly-orogenic basement: U–Pb geochronology of granitoid rocks in the southern Menderes Massif, Western Turkey. *Journal of the Geological Society, London*, **161**, 93–101.

Hill, E.J., Baldwin, S.L. & Lister, G.S. 1992. Unroofing of active metamorphic core complexes in the D'Entrecastaux Islands, Papua New Guinea. *Geology*, **20**, 907–910.

Hinthorne, J.R., Anderson, C.A., Conrad, R.L. & Lovering, J.F. 1979. Single-grain $^{207}Pb/^{206}Pb$ and U/Pb age determinations with a 10 dm spatial resolution using the ion microprobe mass analyser (IMMA). *Chemical Geology*, **25**, 271–303.

Işık, V. & Tekeli, O. 2001. Late orogenic crustal extension in northern Menderes Massif (western Turkey): evidence for metamorphic core complex formation. *International Journal of Earth Sciences*, **89**, 757–765.

Işık, V., Seyitoğlu, G. & Çemen, İ. 2003. Ductile–brittle transition along the Alasehir detachment fault and its structural relationship with the Simav detachment fault, Menderes Massif, western Turkey. *Tectonophysics*, **374**, 1–18.

Işık, V., Tekeli, O. & Seyitoğlu, G. 2004. The $^{40}Ar/^{39}Ar$ age of extensional ductile deformation and granitoid intrusion in the northern Menderes core complex: implications for the initiation of extensional tectonics in western Turkey. *Journal of Asian Earth Sciences*, **89**, 757–765.

John, B.E. & Howard, K.A. 1995. Rapid extension recorded by cooling-age patterns and brittle deformation, Naxos, Greece. *Journal of Geophysical Research*, **100**, 9969–9979.

Kumerics, C., Ring, U., Brichau, S., Régnier, J.-L., Glodny, J. & Monie, P. 2004. The extensional Ikaria shear zone and associated brittle detachments faults, Aegean Sea, Greece. *Journal of the Geological Society, London*, **xxx**, xx–xxx.

Lee, J. & Lister, G.S. 1992. Late Miocene ductile extension and detachment faulting, Mykonos, Greece. *Geology*, **20**, 121–124.

Lister, G.S., Banga, G. & Feenstra, A. 1984. Metamorphic core complexes of Cordilleran type in the Cyclades, Aegean Sea, Greece. *Geology*, **12**, 221–225.

Loos, S. & Reischmann, T. 1999. The evolution of the southern Menderes Massif in SW Turkey as revealed by zircon dating. *Journal of the Geological Society, London*, **156**, 1021–1030.

Oberhänsli, R., Partzsch, J.H., Candan, O. & Çetikaplan, M. 2001. First occurrence of Fe–Mg carpholite documenting a high-pressure metamorphism in metasediments of the Lycian Nappes, SW Turkey. *International Journal of Earth Sciences*, **89**, 867–873.

Ring, U. & Layer, P.W. 2003. High-pressure metamorphism in the Aegean, eastern Mediterranean: sequential accretion from the Late Cretaceous until the Miocene to Recent. *Tectonics*, **22**(3), 1022, doi: 10.1029/2001TC001350.

Ring, U., Gessner, K., Güngör, T. & Passchier, C.W. 1999a. The Menderes Massif of western Turkey and the Cycladic Massif in the Aegean—do they really correlate? *Journal of the Geological Society, London*, **156**, 3–6.

Ring, U., Laws, S. & Bernet, M. 1999b. Structural analysis of a complex nappe sequence and late-orogenic basins from the Aegean Island of Samos, Greece. *Journal of Structural Geology*, **21**, 1575–1601.

Ring, U., Layer, P.W. & Reischmann, T. 2001. Miocene high-pressure metamorphism in the Cyclades and Crete, Aegean Sea, Greece: evidence for large-magnitude displacement on the Cretan detachment. *Geology*, **29**, 395–398.

Ring, U., Johnson, C., Hetzel, R. & Gessner, K. 2003a. Tectonic denudation of a Late Cretaceous–Tertiary collisional belt: regionally symmetric cooling patterns and their relation to extensional faults in the Anatolide belt of western Turkey. *Geological Magazine*, **140**, 421–441.

Ring, U., Thomson, S.N. & Bröcker, M. 2003b. Fast extension but little exhumation: the Vari detachment in the Cyclades, Greece. *Geological Magazine*, **140**, 245–252.

Şengör, A.M.C. 1987. Cross faults and differential stretching in their hanging walls in regions of low-angle normal faulting: examples from western Turkey. *In:* Coward, M.J., Dewey, J.F. & Hancock, P.L. (eds) *Continental Extensional Tectonics*. Geological Society, London, Special Publications, **28**, 405–473.

Seyitoğlu, G. 1997. The Simav graben: an example of young E–W trending structures in the late Cenozoic extensional system of western Turkey. *Turkish Journal of Earth Sciences*, **6**, 135–141.

Seyitoğlu, G., Scott, B. & Rundle, C.C. 1992. Timing of Cenozoic extensional tectonics in west Turkey. *Journal of the Geological Society, London*, **149**, 533–538.

Seyitoğlu, G., Çemen, İ. & Tekeli, O. 2000. Extensional folding in the Alasehir (Gediz) graben, western Turkey. *Journal of the Geological Society, London*, **157**, 1097–1100.

Seyitoğlu, G., Tekeli, O., Çemen, İ., Sen, S. & Işık, V. 2002. The role of flexural rotation/rolling hinge model in the tectonic evolution of the Alasehir graben, western Turkey. *Geological Magazine*, **139**, 15–26.

Sherlock, S., Kelley, S., Inger, S., Harris, N. & Okay, A. 1999. $^{40}Ar–^{39}Ar$ and Rb–Sr geochronology of high-pressure metamorphism and exhumation history of the Tavsanli Zone, NW Turkey. *Contributions to Mineralogy and Petrography*, **137**, 46–58.

Stacey, F.S. & Kramers, J.D. 1975. Approximation of terrestrial lead isotope evolution by two-stage model. *Earth and Planetary Science Letters*, **26**, 207–221.

Thomson, S.N., Stöckhert, B. & Brix, M.A. 1999. Miocene high-pressure metamorphic rocks of Crete, Greece: rapid exhumation by buoyant escape. *In:* Ring, U., Brandon, M.T., Lister, G.S. & Willett, S.D. (eds) *Exhumation Processes: Normal Faulting, Ductile Flow and Erosion*. Geological Society, London, Special Publications, **154**, 87–108.

Received 30 January 2004; revised typescript accepted 2 October 2004.
Scientific editing by Martin Whitehouse